




# CKAMP44 controls synaptic function and strength of relay neurons during early development of the dorsal lateral geniculate nucleus

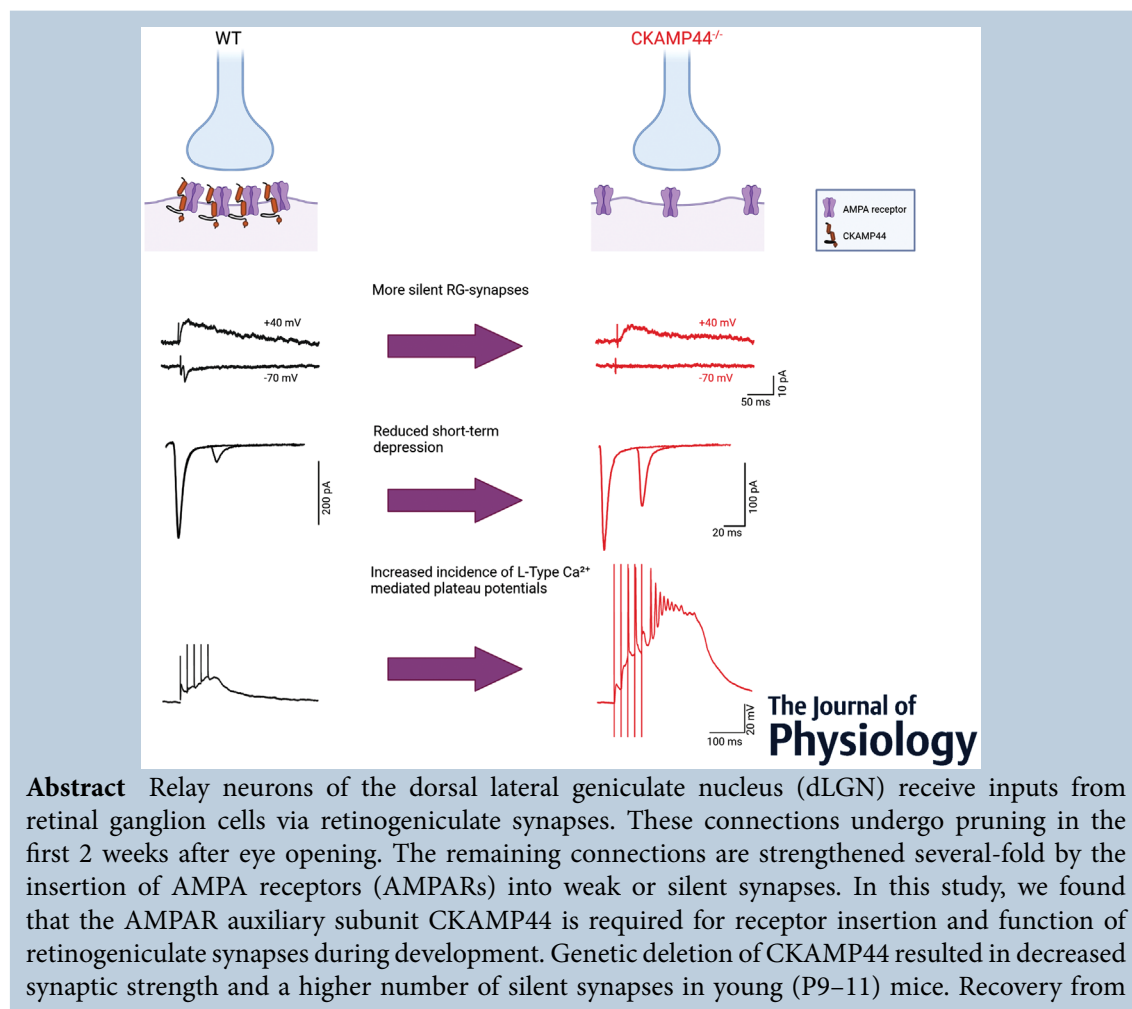
Florian Hetsch<sup>1</sup> , Danni Wang<sup>1</sup> , Xufeng Chen<sup>1</sup>, Jiong Zhang<sup>1</sup>, Muhammad Aslam<sup>1</sup>, Marcel Kegel<sup>1</sup>, Henrik Tonner<sup>2</sup>, Franz Grus<sup>2</sup> and Jakob von Engelhardt<sup>1</sup> 

<sup>1</sup>Institute of Pathophysiology, Focus Program Translational Neurosciences (FTN), University Medical Center of the Johannes Gutenberg University Mainz, Mainz, Germany

<sup>2</sup>Experimental Ophthalmology, University Medical Center of the Johannes Gutenberg University Mainz, Mainz, Germany

Handling Editors: David Wyllie & Jian Shi

The peer review history is available in the Supporting Information section of this article (<https://doi.org/10.1113/JP283172#support-information-section>).



F. Hetsch, D. Wang, and X. Chen contributed equally to this work.

desensitisation of AMPARs was faster in CKAMP44 knockout (CKAMP44<sup>-/-</sup>) than in wild-type mice. Moreover, loss of CKAMP44 increased the probability of inducing plateau potentials, which are known to be important for eye-specific input segregation and retinogeniculate synapse maturation. The anatomy of relay neurons in the dLGN was changed in young CKAMP44<sup>-/-</sup> mice showing a transient increase in dendritic branching that normalised during later development (P26–33). Interestingly, input segregation in young CKAMP44<sup>-/-</sup> mice was not affected when compared to wild-type mice. These results demonstrate that CKAMP44 promotes maturation and modulates function of retinogeniculate synapses during early development of the visual system without affecting input segregation.

(Received 6 April 2022; accepted after revision 27 June 2022; first published online 30 June 2022)

**Corresponding author** J. von Engelhardt: Institute of Pathophysiology, Focus Program Translational Neurosciences (FTN), University Medical Center of the Johannes Gutenberg University Mainz, Duesbergweg 6, Mainz 55128, Germany. Email: engelhardt@uni-mainz.de

**Abstract figure legend** AMPA receptor auxiliary subunit CKAMP44 influences synaptic function in retinogeniculate synapses of young mice. CKAMP44 unsilences synapses by recruiting AMPA receptors to the synapse. Furthermore, genetic deletion of CKAMP44 reduces short-term depression and increases the probability of eliciting L-type Ca<sup>2+</sup> channel-mediated plateau potentials.

### Key points

- Expression of CKAMP44 starts early during development of the dorsal lateral geniculate nucleus (dLGN) and remains stable in relay neurons and interneurons.
- Genetic deletion of CKAMP44 decreases synaptic strength and increases silent synapse number in dLGN relay neurons; increases the rate of recovery from desensitisation of AMPA receptors in dLGN relay neurons; and reduces synaptic short-term depression in retinogeniculate synapses.
- The probability of inducing plateau potentials is elevated in relay neurons of CKAMP44<sup>-/-</sup> mice.
- Eye-specific input segregation is unaffected in the dLGN of CKAMP44<sup>-/-</sup> mice.
- Deletion of CKAMP44 mildly affects dendritic arborisation of relay neurons in the dLGN.

## Introduction

The establishment of synaptic connections during development is a well-orchestrated process that has been extensively studied specifically in the visual system (Huberman et al., 2008). Retinal ganglion cells excite relay neurons of the dorsal lateral geniculate nucleus (dLGN)

via retinogeniculate synapses. In the first postnatal week, each relay neuron receives weak inputs from many retinal ganglion cells. Most retinogeniculate synapses are pruned with development and the surviving synapses increase their strength approximately 60-fold (Chen & Regehr, 2000; Litvina & Chen, 2017a). This strengthening and refinement of retinogeniculate synapses requires insertion

**Florian Hetsch** did his doctoral studies at the MDC in Berlin and is a post-doctoral researcher at the Institute for Pathophysiology of the University Medical Centre of the Johannes Gutenberg University Mainz. His research interest lies in the visual system with emphasis on the synaptic properties of the retinogeniculate synapse. **Danni Wang** obtained her MD at Heidelberg University followed by doctoral research in physiology. During her doctoral study, her research aimed at investigating the development and homeostatic plasticity of the retinogeniculate synapse. She is currently a doctor in the department of neonatology in Shanghai Children's Hospital. Her major interests focus on the pathophysiology of neural injury caused by intra-uterine growth restriction. **Xufeng Chen** finished his PhD at Heidelberg University. He is currently a senior postdoctoral associate in the State University of New York at Stony Brook. His current research focuses on synaptic plasticity and signal transmission under chronic pain.



of AMPA receptors (AMPA) into weak or silent synapses (i.e. synapses that contain NMDA receptors, but not AMPARs) (Chen & Regehr, 2000). Retinal ganglion cells from both eyes send their input initially to overlapping areas of each dLGN. The inputs segregate after birth such that the centre of the mouse dLGN receives input from the ipsilateral retina and the remaining part from the contralateral retina (Guido, 2018; Litvina & Chen, 2017b). Early-stage eye-specific segregation depends on spontaneous retinal activity (Penn et al., 1998; Torborg et al., 2005). In the following developmental stage, visual experience and excitatory input to the dLGN are necessary for the maintenance of refined retinogeniculate connections (Hooks & Chen, 2006). Importantly, high frequency bursts (>10 Hz) of activity are particularly efficient in driving input segregation (Torborg et al., 2005). Moreover, depolarisation-induced activation of L-type  $\text{Ca}^{2+}$  channel activity causing plateau potentials is required for input segregation (Dilger et al., 2015).

AMPA complexes contain auxiliary subunits that control surface targeting, synaptic anchoring and gating of AMPARs (Jacobi & von Engelhardt, 2017). Genetic deletion of the auxiliary subunit TARP  $\gamma$ -2, for instance, affects the late phase refinement and experience-dependent plasticity of retinogeniculate synapses (Louros et al., 2014). In a recent study, the auxiliary subunit CKAMP44 has been described as playing a pivotal role in controlling retinogeniculate synapse function of adult mice (Chen et al., 2018). However, whether CKAMP44 is involved in the development of dLGN relay neurons and retinogeniculate synapse function in young mice is unknown.

We here show that CKAMP44 is expressed in dLGN relay neurons and interneurons throughout development. Moreover, using electrophysiological techniques we demonstrate that CKAMP44 affects synapse strength and function as well as the number of silent synapses in the first postnatal weeks. Furthermore, CKAMP44 controls L-type  $\text{Ca}^{2+}$  channel-mediated plateau potential initiation. Anatomical analyses reveal changes in the development of relay neuron morphology but not in input segregation in the dLGN of CKAMP44<sup>-/-</sup> mice.

## Methods

### Ethical approval

All experiments using mice complied with the principles and regulations of *The Journal of Physiology* with respect to reporting animal experiments (Grundy, 2015). They were performed according to the German Animal Welfare Act and approved by the Governmental Supervisory Panel on Animal Experiments of Rhineland-Palatinate (Approval Number: G20-1-147). Mice were born and raised in-house

in the Translational Animal Research Centre (TARC) of the University Medicine of Mainz in cages with free access to food and water under a 12 h light–12 h dark cycle. One hundred and seven mice of either sex were used in this study.

### Fluorescence *in situ* hybridisation

All solutions for fluorescence *in situ* hybridisation (FISH) experiments were prepared with MilliQ water treated with diethylpyrocarbonate (DEPC). Brains from P5–7, P15–17, P26–33 and P60–90 mice were harvested in DEPC-treated MilliQ water and frozen on a metal tray submerged in liquid nitrogen to ensure mRNA stability. Tissue was stored at  $-80^{\circ}\text{C}$  for further processing. Reagents for FISH were obtained from Thermo Fisher Scientific and FISH labelling was performed on 12  $\mu\text{m}$ -thick coronal brain cryosections containing dLGN using brain atlases for developing and adult mouse brains as reference (Paxinos & Franklin, 2012; Paxinos et al., 2006). The cryosections were mounted on Superfrost plus slides (Thermo Fisher Scientific) and were fixed in 4% paraformaldehyde (PFA) overnight. Slides were then dehydrated in an increasing ethanol series and dried at  $60^{\circ}\text{C}$  for 1 h. Cryosections were rehydrated in phosphate-buffered saline (PBS) before FISH labelling, which was performed according to the manufacturer's protocol (Thermo Fisher Scientific, ViewRNA ISH Assay). Briefly, cryosections were subjected to limited protease digestion using Protease (QVC0511) diluted 1:100 in  $1\times$  PBS. Following a 5 min Protease QS treatment, cryosections were washed. The permeabilised (protease-treated) cryosections were co-hybridised for 6 h at  $40^{\circ}\text{C}$  in probe-containing solution (proprietary ViewRNA ISH probe sets for murine *Shisa9*, VB1-19 976 and *Gad1*, VB4-19 846, diluted 1:40 in Probe Set Diluent QF, QVC0512). Following the probe hybridisation, cryosections were washed and then subjected to sequential hybridisation at  $40^{\circ}\text{C}$  for 30 min with PreAmplifier Mix, Amplifier Mix and Label Probe Mix (*Shisa9*, Alexa Fluor 546; *Gad1*, Alexa Fluor 488), each reagent diluted 1:100 in the provided diluent. Sequential hybridisation was interspersed and followed by washing steps. Sections were then incubated in 4',6-diamidino-2-phenylindole (DAPI) solution ( $100\times$  DAPI diluted 1:100 in PBS). The slides were washed and air-dried for a few minutes before mounting with ProLong Gold Antifade Mountant (Thermo Fisher Scientific).

### Brain slices preparation for electrophysiology

Acute brain slices containing the dLGN for electrophysiological experiments were collected as described previously (Chen et al., 2019; Turner & Salt, 1998). Briefly, anaesthetised mice were decapitated and brains

were removed and quickly immersed in oxygenated 4°C choline-based solution containing (in mM): 87 NaCl, 2.5 KCl, 37.5 choline chloride, 25 NaHCO<sub>3</sub>, 1.25 NaH<sub>2</sub>PO<sub>4</sub>, 25 glucose, 0.5 CaCl<sub>2</sub> and 7 MgCl<sub>2</sub>. Brain slices of 250 μm were cut on a vibratome (Leica VT1200, Leica Microsystems, Wetzlar, Germany); 300 μm slices were generated for evoked plateau potentials in an oxygenated 4°C sucrose-based cutting solution containing (in mM): 212 sucrose, 3 KCl, 26 NaHCO<sub>3</sub>, 1.25 NaH<sub>2</sub>PO<sub>4</sub>, 10 glucose, 0.5 CaCl<sub>2</sub> and 7 MgCl<sub>2</sub>. Sagittal slices were obtained for miniature excitatory postsynaptic current (mEPSC) recordings. To preserve intact retinogeniculate fibres for evoked excitatory postsynaptic current (EPSC) recordings, the two hemispheres were separated with an angle of 3–5° to the sagittal plane and an angle of 10–25° outwards in the mediolateral plane during slicing. The slices were collected in oxygenated choline-based solution at 34°C for 25 min for recovery and then transferred to artificial cerebrospinal fluid (ACSF) containing (in mM): 125 NaCl, 25 NaHCO<sub>3</sub>, 1.25 NaH<sub>2</sub>PO<sub>4</sub>, 2.5 KCl, 2 CaCl<sub>2</sub>, 1 MgCl<sub>2</sub> and 25 glucose at 34°C for another 25 min. Slices were kept at room temperature for about 30 min before recording.

### **In vitro electrophysiology**

Whole-cell patch clamp recordings were performed at room temperature. Pipettes were pulled from borosilicate glass capillaries with a resistance of 3–5 MΩ. Patch pipettes were filled with intracellular solution containing (in mM): 120 caesium gluconate, 10 CsCl, 8 NaCl, 10 HEPES, 10 phosphocreatine-Na, 0.3 GTP, 2 Mg<sup>2+</sup>-ATP and 0.2 EGTA (pH 7.3, adjusted with CsOH). mEPSC recordings were performed as described previously (von Engelhardt et al., 2008) at the holding potential of –70 mV with 50 μM D-2-amino-5-phosphonovaleric acid (D-APV) (Sigma-Aldrich, Taufkirchen, Germany), 10 μM SR 95531 hydrobromide (gabazine) (Sigma-Aldrich) and 1 μM tetrodotoxin (TTX) (Biotrend, Cologne, Germany) in the ACSF to block NMDA receptors (NMDARs), γ-aminobutyric acid type A (GABA<sub>A</sub>) receptors and voltage-gated Na<sup>+</sup> channels, respectively. mEPSC data were analysed with the help of clampfit software (version 10.2.0.13, MDS Analytical Technologies, Sunnyvale, CA, USA) together with the *minianalysis* plugin using a template-matching algorithm.

For evoked EPSC recordings, patch pipettes were filled with intracellular solution containing (in mM): 35 caesium gluconate, 100 CsCl, 10 HEPES, 10 EGTA, and 0.1 D-600 (pH 7.3, adjusted with CsOH). Paired-pulse ratio recordings were performed at a holding potential of –70 mV in the presence of 50 μM APV and 10 μM gabazine. Paired-pulse stimuli of the optic tract were applied with 30, 100, 300, 1000 and 3000 ms

inter-stimulus intervals. Paired-pulse ratios of current amplitudes (EPSC2/EPSC1) were calculated from the means of 20 EPSC pairs.

AMPA/NMDA ratios were calculated from the amplitudes of AMPAR-mediated and NMDAR-mediated currents that were recorded at a holding potential of –70 and +40 mV, respectively. NMDAR-mediated current amplitudes were measured 25 ms after the start of the stimulus artefact. Ten micromolar gabazine was used to block GABA<sub>A</sub> receptors.

Silent fibre recordings were performed in the presence of gabazine. Cells were initially held at +40 mV to record NMDAR-mediated currents. A weak optic tract stimulation was applied and the stimulus intensity was gradually increased until a postsynaptic response was observed. Once a minimal NMDAR-mediated current was observed, the holding potential was switched to –70 mV to record AMPAR-mediated currents. Stimulation of a silent fibre elicits NMDAR- but not AMPAR-mediated currents. We then recorded NMDAR-mediated currents at +40 mV once more to control for potential movements of slice or stimulation pipette that could explain the absence of AMPAR-mediated currents.

For the analysis of L-type calcium channel-mediated plateau potentials, patch pipettes were filled with intracellular solution containing (in mM): 140 potassium gluconate, 10 HEPES, 2 Mg-ATP salt, 0.3 NaCl, and 0.1 Na-GTP salt (pH 7.25, adjusted with KOH). Whole-cell current clamp recordings were performed in artificial cerebrospinal fluid (ACSF) containing (in mM): 125 NaCl, 25 NaHCO<sub>3</sub>, 1.25 NaH<sub>2</sub>PO<sub>4</sub>, 2.5 KCl, 2 CaCl<sub>2</sub>, 2 MgCl<sub>2</sub>, 10 glucose at 32 to 34°C. To evoke synaptic activity, we adopted methods described previously (Dilger et al., 2015). Briefly, square pulses (0.1 ms duration) were delivered at 50 Hz by a monopolar electrode placed in the optic tract connected to a stimulus isolator (A365, World Precision Instruments, Sarasota, FL, USA) that was controlled through Patchmaster software. Stimulation was repeated 10 times and responses averaged. To ensure similar stimulation regimes, the stimulation intensity was kept at a similar strength for both genotypes (median wild type *vs.* CKAMP44<sup>-/-</sup>: 350 *vs.* 353 μA). Plateau potentials were classified by their characteristic appearance (Dilger et al., 2015; Lo et al., 2002), e.g. their long-lasting duration (100–500 ms), high amplitude (40–60 mV) and bursts of inactivating sodium spikes. The area of the evoked responses and number of inactivating sodium spikes (>1 mV in amplitude) of plateau potentials were analysed using IGOR Pro 6.37 with Neuromatic extension (WaveMetrics Inc., Lake Oswego, OR, USA).

Nucleated patch experiments were performed as described (Sather et al., 1992) using theta glass tubing mounted onto a piezo actuator. Application pipettes were tested by perfusing solutions with different salt

concentrations through the two barrels onto open patch pipettes and recording current changes with 1 ms transitions of the application pipette. Only application pipettes with 20–80% rise times below 120  $\mu$ s and with a reasonable symmetrical on- and offset were used. The application solution contained (in mM): 135 NaCl, 10 HEPES, 5.4 KCl, 1.8 CaCl<sub>2</sub>, 1 MgCl<sub>2</sub>, 5 glucose (pH 7.2). AMPAR-mediated currents were evoked by applying 1 ms glutamate (1 mM) pulses onto nucleated patches of relay neurons.

### Biocytin filling and labelling

Brain slices of mice were prepared as for electrophysiological experiments. Filling of neurons was performed as described previously (Muller et al., 2018). Briefly, relay neurons were patch-clamped for 15 min with an intracellular recording solution containing 0.1–0.5% biocytin (Sigma-Aldrich; the solution was sonicated for 30 min before use). After biocytin filling, slices were transferred into 4% PFA in PBS at 4°C overnight. Brain slices were washed with 1 $\times$  PBS for 10 min (3 times) and then incubated in a blocking solution (containing 0.2% Triton X-100 and 5% bovine serum albumin in PBS) on an orbital shaker for 2 h at room temperature. The blocking solution was afterwards replaced by a solution containing streptavidin-Alexa 488 or 568 (1:1000 in PBS) (Thermo Fisher Scientific). Slices were incubated in the streptavidin solution on an orbital shaker at 4°C overnight. Light exposure was avoided during subsequent washing steps (with 1 $\times$  PBS for 10 min (3 times) and rinsed with tap water). Before mounting, slices were imaged with a fluorescence microscope to ensure that the biocytin-filled neurons were on the upper side of the slices.

### Eye-specific input segregation

Mice aged P9–11 were analgised with buprenorphine and anaesthetised with isoflurane. For an anterograde labelling of retinal ganglion axons, 1  $\mu$ l of cholera toxin B (CTB) subunit conjugated to Alexa Fluor 488 (green) and Alexa Fluor 594 (red) (Thermo Fisher Scientific) was intravitreally injected into the right and left eye, respectively. CTB was dissolved in PBS yielding a concentration of 1  $\mu$ g/ $\mu$ l. After 48 h, animals were subcutaneously injected with a ketamine–xylazine cocktail (200 mg/kg and 20 mg/kg body weight) and transcardially perfused with 1 $\times$  PBS and subsequently ice-cold 4% PFA. Brains were removed and fixed in 4% PFA at 4°C overnight. After three washing steps with 1 $\times$  PBS for 10 min, brains were sectioned coronally (thickness, 70  $\mu$ m) using a vibratome. Brain sections were mounted onto slides using ProLong

Gold Antifade Mountant (Thermo Fisher Scientific) and stored at room temperature for further processing.

### Imaging and analyses

Imaging for FISH experiments and segregation analysis was performed on a Leica TCS SP5 confocal microscope using a HCX PL APO CS  $\times$ 20.0 (NA = 0.70) dry UV objective. Expression of *Shisa9* mRNA (encoding CKAMP44) was quantified in relay neurons and interneurons by counting red dots per cell. Fiji software (version 2.0.2) was used to enhance contrast and count dots. Theoretically, each dot reflects one mRNA molecule (Trcek et al., 2011). Interneurons were identified by the presence of green signal (indicating presence of *Gad1* mRNA).

For the acquisition of eye-specific inputs, fluorescence intensities for CTB–Alexa 488 and 594 were adjusted using the look-up table provided by the Leica TCS SP5 acquisition software to avoid under- or overexposure of images. Laser intensities were adjusted accordingly. To quantify input segregation, a threshold-independent method introduced by Torborg and Feller (Torborg & Feller, 2004) was used. Briefly, for each mouse, three to five consecutive slices containing the largest contralateral-dominant area were used for analysis. Analysis was done using Fiji software. First, a region of interest was selected encompassing the dLGN. The image was subjected to background subtraction using a rolling ball radius of 200 pixels. Then the logarithm of the ratio of fluorescence intensities of the dyes that were injected into the ipsilateral and contralateral eye ( $R = \log [F_I/F_C]$ ) was calculated for each image and each pixel of the dLGN. Mean  $R$ -values were calculated for each mouse. The obtained  $R$ -values were between  $-2$  and  $+2$ .  $R$ -values close to  $-2$  indicate strong input from the contralateral eye, while  $R$ -values close to  $+2$  suggest the dominant input stems from the ipsilateral eye.  $R$ -values close to zero reflect similar Alexa Fluor 488 and Alexa Fluor 594 fluorescence signal intensity in the given pixels. The variance of the  $R$ -distribution correlates with the extent of input segregation.

Confocal images of P9–11 relay neurons for morphological analysis were obtained using a Zeiss LSM 710 confocal microscope with an EC Plan-Neofluar  $\times$ 40/1.30 Oil DIC objective and Zen 2.3 software (Carl Zeiss, Oberkochen, Germany). Z-stacks of 1  $\mu$ m thickness were acquired. Relay neurons were traced using NeuronStudio software (Version 0.9.92, Computational Neurobiology and Imaging Center Mount Sinai School of Medicine, NY, USA), and Sholl analysis was performed and total dendritic length calculated. Dendritic complexity was investigated by quantifying number of dendrite intersections and number of

branch points with a 10  $\mu\text{m}$  interval for all relay neurons.

Fiji software (version 2.0.2) was used to process images for figures.

## Statistics

We performed statistical comparisons using unpaired two-tailed Student's *t*-test or Mann–Whitney *U*-test depending on whether data were normally distributed, which was confirmed by Kolmogorov–Smirnov (KS) test. For group analysis, one-way ANOVA (CKAMP44 FISH mRNA data) or two-way ANOVA (Sholl analysis data) was performed. Throughout this study, data are shown as means  $\pm$  standard deviation (SD) for normally distributed data or medians and interquartile range (IQR; 25–75%) for non-normally distributed data and the number of cells (*n*) and animals (*N*) are indicated. Data for silent fibre and plateau potential analyses are reported as animal averages. Cumulative distribution of dendrite intersections and branch points was tested for significant changes by a Kolmogorov–Smirnov test (tests performed on pooled single cell data). Statistical analysis was performed using GraphPad Prism (version 9.3.0, GraphPad Software Inc., San Diego, CA, USA) and IGOR Pro 6.37 (WaveMetrics Inc., Lake Oswego, OR, USA). *P*-values  $<0.05$  were considered statistically significant (\**P*  $<0.05$ , \*\**P*  $<0.01$ , \*\*\**P*  $<0.001$ ).

## Results

### CKAMP44 is stably expressed in the dLGN throughout development

Remodelling of the excitatory inputs of dLGN relay neurons with pruning of the majority and strengthening of the remaining retinogeniculate synapses is a crucial step in the development of the visual system (Chen & Regehr, 2000). As AMPAR auxiliary subunit CKAMP44 plays a pivotal role in modulating retinogeniculate synapse function in adult mice (Chen et al., 2018), we wondered whether CKAMP44 is expressed in the dLGN during development and controls the strengthening of relay neuron synapses. To investigate expression of CKAMP44, we performed FISH experiments and showed that *Shisa9* mRNA, which encodes murine CKAMP44, is present in dLGN relay neurons already early during development (P5–7:  $17.21 \pm 2.58$  dots/cell, *n* = 34 cells, *N* = 3 mice, mean  $\pm$  SD) and remained stably expressed throughout development of the dLGN (P15–17:  $18.83 \pm 3.46$  dots/cell, *n* = 36 cells, *N* = 3 mice; P26–33:  $17.23 \pm 2.98$  dots/cell, *n* = 26 cells, *N* = 3 mice; P60–90:  $17.38 \pm 3.31$  dots/cell, *n* = 24 cells, *N* = 3 mice, mean  $\pm$  SD) (Fig. 1A and C).

Absence of *Shisa9* signal in slices from CKAMP44<sup>-/-</sup> mice proved the specificity of the probe (Fig. 1B). Co-hybridisation with a *Gad1* probe, which marks GAD67-positive neurons, showed a lower but stable

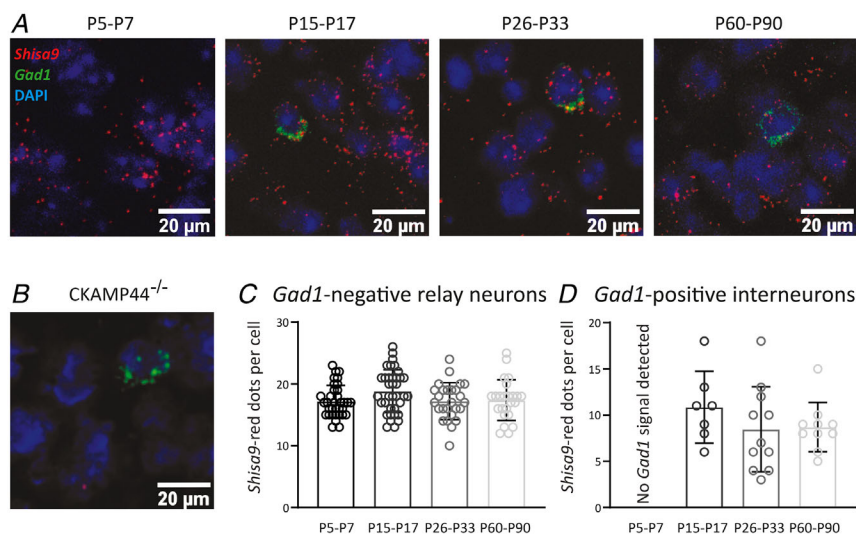


**Figure 1. Developmental profile of CKAMP44 expression in relay neurons and interneurons**  
 A, example FISH images of the dLGN from different age groups co-hybridised with *Shisa9* and *Gad1* FISH probes. Cell nuclei were visualised with DAPI (blue signal). Red signal represents *Shisa9* mRNA and green signal represents *Gad1* mRNA. B, no *Shisa9* signal was detected in the dLGN of CKAMP44<sup>-/-</sup> mice (*N* = 1). C, the expression of *Shisa9* in *Gad1*-negative relay neurons quantified as the number of red dots per cell (*n* = 34 neurons, *N* = 3 mice for P5–7, *n* = 36 neurons, *N* = 3 mice for P15–17, *n* = 26 neurons, *N* = 3 mice for P26–33 and *n* = 24 neurons, *N* = 3 mice for P60–90, mean  $\pm$  SD). D, the expression of *Shisa9* mRNA in *Gad1*-positive interneurons quantified as the number of red dots in cells that are positive for green signal (*n* = 7 relay neurons for P15–17 mice, 11 relay neurons for P26–33 mice and 10 relay neurons for P60–90 mice, mean  $\pm$  SD, *N* = 3 animals per age group). [Colour figure can be viewed at wileyonlinelibrary.com]

expression of *Shisa9* mRNA in *Gad1*-positive neurons (P15–17:  $10.86 \pm 3.89$  dots/cell,  $n = 7$  cells,  $N = 3$  mice; P26–33:  $8.46 \pm 4.61$  dots/cell,  $n = 11$  cells,  $N = 3$  mice; P60–90:  $8.70 \pm 2.67$  dots/cell,  $n = 10$  cells,  $N = 3$  mice, mean  $\pm$  SD) (Fig. 1A and D). *Gad1*-positive neurons were not detected in the dLGN of P5–7 mice (Fig. 1A). These data suggest that CKAMP44 is stably expressed in relay neurons and interneurons throughout development of the dLGN, indicating a role of CKAMP44 starting from an early stage of development.

### CKAMP44 affects synaptic strength and plasticity during development of the dLGN

To investigate whether the number of synaptic AMPARs is controlled by CKAMP44 during development of the dLGN, AMPA/NMDA ratios were quantified in retinogeniculate synapses of P9–11 wild-type and CKAMP44<sup>-/-</sup> mice. The analysis of AMPA/NMDA ratios allows estimation of the number of AMPARs at functional synapses from the amplitude of AMPAR-mediated currents normalised to the amplitude of NMDAR-mediated currents. AMPA/NMDA ratios were reduced by approximately 33% (Wild-type:  $0.4459 [0.3353-0.8185]$ ,  $n = 27$  neurons,  $N = 4$  mice; CKAMP44<sup>-/-</sup>:  $0.2964 [0.1907-0.5464]$ ,  $n = 27$  neurons,  $N = 5$  mice, Mann–Whitney test:  $P = 0.0074$ , median [IQR]) in retinogeniculate synapses of P9–11 CKAMP44<sup>-/-</sup> mice (Fig. 2B and C). This suggests that CKAMP44 increases synaptic AMPAR number in retinogeniculate synapses of young relay neurons.

The previous results were corroborated by decreased mEPSC amplitudes in dLGN relay neurons of P5–P7 and P9–P11 CKAMP44<sup>-/-</sup> mice (Wild-type, P5–7:  $15.12 \pm 1.93$  pA,  $n = 23$  neurons,  $N = 4$  mice; CKAMP44<sup>-/-</sup>, P5–7:

$13.29 \pm 1.72$  pA,  $n = 27$  neurons,  $N = 5$  mice,  $t$ -test:  $P = 0.0009$ , mean  $\pm$  SD; Wild-type, P9–11:  $14.91 \pm 2.51$  pA,  $n = 37$  relay neurons,  $N = 7$  mice; CKAMP44<sup>-/-</sup>, P9–11:  $13.68 \pm 2.67$  pA,  $n = 39$ ,  $N = 6$  mice,  $t$ -test:  $P = 0.0432$ , mean  $\pm$  SD). The amplitude reduction suggests that the AMPAR number per synapse is reduced in relay neurons of P5–7 and P9–11 CKAMP44<sup>-/-</sup> mice (Fig. 3A and B). Interestingly, the deletion of CKAMP44 also affected mEPSC frequency, which was lower (Wild-type:  $0.886 [0.435-1.874]$  Hz,  $n = 37$  relay neurons,  $N = 7$  mice; CKAMP44<sup>-/-</sup>:  $0.5063 [0.211-0.957]$  Hz,  $n = 39$  relay neurons,  $N = 6$  mice, Mann–Whitney test:  $P = 0.0204$ , median [IQR]) in relay neurons of P9–11 CKAMP44<sup>-/-</sup> mice than in wild-type mice (Fig. 3B). A similar reduction in mEPSC frequency was observed in juvenile and adult CKAMP44<sup>-/-</sup> mice (data not shown). A possible explanation for the reduced mEPSC frequency in relay neurons of CKAMP44<sup>-/-</sup> mice is that the accompanied reduction in mEPSC amplitude prevents the detection of small mEPSCs near the noise level. However, a reduction in mEPSC frequency may also result from a reduction in structural synapse number or an increase in silent synapse number, i.e. synapses that are devoid of AMPARs, but contain NMDARs.

To quantify silent synapse number in dLGN relay neurons we performed minimal stimulation experiments. An increase in silent synapse number augments the likelihood that silent fibres are observed in such an experiment. Retinogeniculate fibres establish synapses with approximately 120–250 release sites with LGN relay neurons of adult mice (Chen & Regehr, 2000). Consistent with the high number of release sites, silent retinogeniculate fibres were not found in adult mice (Chen & Regehr, 2000). However, silent fibres can be observed with minimal stimulation experiments at earlier developmental time points, at which each

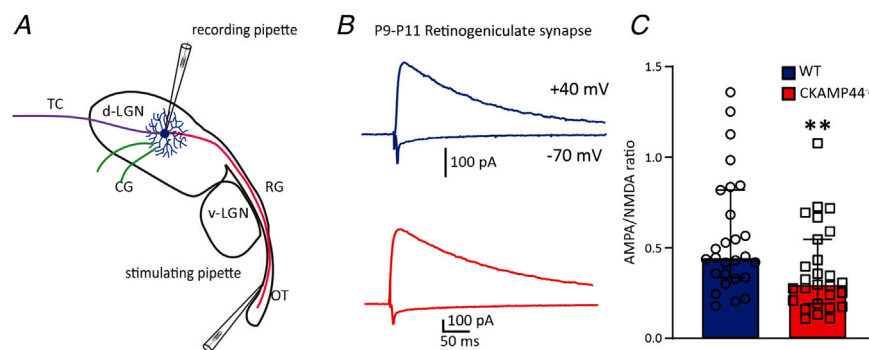


**Figure 2. CKAMP44 increases synapse strength in P9–11 mice**

A, schematic representation of stimulation of retinogeniculate synapses (CG, corticogeniculate fibres, green; OT, optic tract; RG, retinogeniculate fibres, red; TC, thalamocortical fibres, purple). B, examples of AMPAR- and NMDAR-mediated currents. Wild-type traces in blue, CKAMP44<sup>-/-</sup> in red. C, deletion of CKAMP44 reduces the AMPA/NMDA ratio in retinogeniculate synapses (C). C,  $n = 27$  relay neurons recorded from  $N = 4$  wild-type mice and  $n = 27$  relay neurons from  $N = 5$  CKAMP44<sup>-/-</sup> mice at age P9–11, respectively; median and IQR. [Colour figure can be viewed at [wileyonlinelibrary.com](http://wileyonlinelibrary.com)]

retinogeniculate fibre has only a few release sites (Chen & Regehr, 2000). The percentage of silent retinogeniculate fibres was significantly higher in P9–11 CKAMP44<sup>-/-</sup> mice compared to wild-type mice (Wild-type: 17.15% [0.00–31.23%],  $N = 12$  mice; CKAMP44<sup>-/-</sup>: 50.00% [15.00–61.68%],  $N = 14$  mice, Mann–Whitney test:  $P = 0.0217$ , median [IQR]) (Fig. 4A–C).

AMPA/NMDA ratio quantified for silent and non-silent fibres together was not significantly reduced in relay neurons of CKAMP44<sup>-/-</sup> mice (Wild-type: 0.289 [0.172–0.492],  $N = 12$  mice; CKAMP44<sup>-/-</sup>: 0.202 [0.104–0.315],  $N = 14$  mice, Mann–Whitney test:  $P = 0.1308$ , median [IQR]) but showed a trend for reduction (Fig. 4D, upper panel). The magnitude of the trend for reduction in the AMPA/NMDA ratio was comparable to

the reduction in AMPA/NMDA ratio in experiments where many retinogeniculate fibres were activated simultaneously (Fig. 2). The AMPA/NMDA ratio of only non-silent fibres was not significantly different between genotypes (Wild-type:  $0.410 \pm 0.181$ ,  $N = 12$  mice; CKAMP44<sup>-/-</sup>:  $0.377 \pm 0.148$ ,  $N = 14$  mice,  $t$ -test:  $P = 0.6127$ , mean  $\pm$  SD) (Fig. 4D, lower panel). This suggests that non-silent retinogeniculate synapses of P9–11 CKAMP44<sup>-/-</sup> mice contain normal numbers of AMPARs and that the reduction of the AMPA/NMDA ratio results mainly from the increased number of silent fibres. This finding would also explain the significant reduction in mEPSC frequency, but comparably small reduction in mEPSC amplitude in relay neurons of P9–11 CKAMP44<sup>-/-</sup> mice.

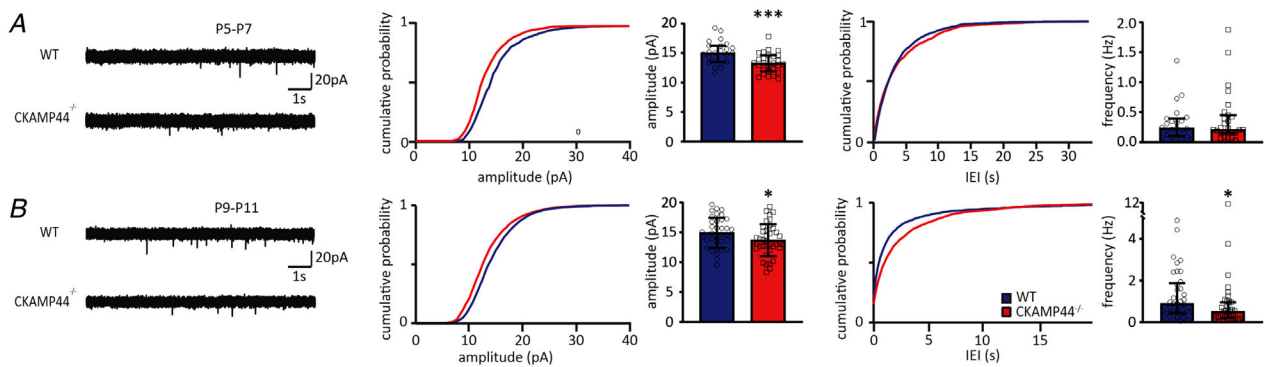


**Figure 3. CKAMP44 affects mEPSCs of dLGN relay neuron in early development**

Left, example traces of mEPSCs from P5–7 (A) and P9–11 (B) wild-type and CKAMP44<sup>-/-</sup> relay neurons. Right, cumulative distribution of mEPSC amplitudes and inter-event intervals (IEIs) from P5–7 (A) and P9–11 (B) mice and bar plots showing the quantification of mEPSC amplitude and frequency.  $n = 23$  relay neurons and  $n = 27$  relay neurons recorded from  $N = 4$  wild-type and  $N = 5$  CKAMP44<sup>-/-</sup> mice at P5–7;  $n = 37$  relay neurons and  $n = 39$  relay neurons recorded from  $N = 7$  wild-type mice and  $N = 6$  CKAMP44<sup>-/-</sup> mice at P9–11. Data shown as mean  $\pm$  SD for amplitudes and median and IQR for frequencies. [Colour figure can be viewed at wileyonlinelibrary.com]

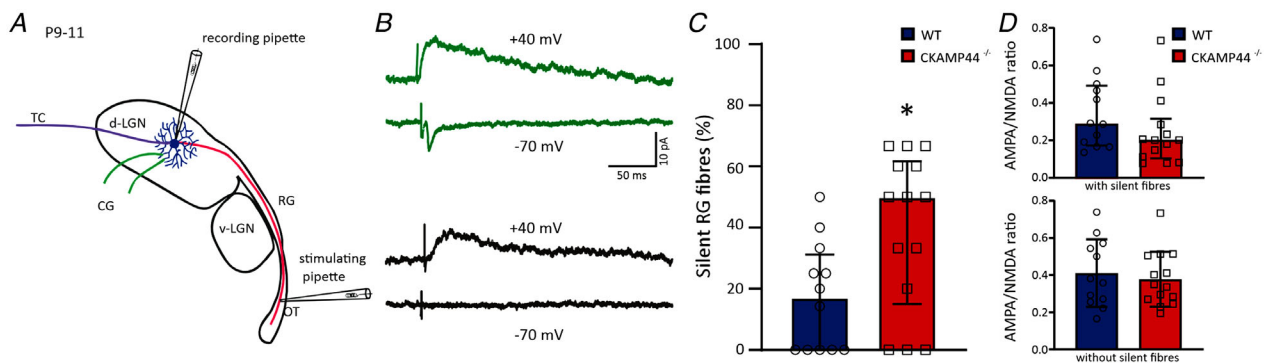


**Figure 4. CKAMP44 decreases the number of silent fibres**

A, schematic representation of silent fibre analysis (CG, corticogeniculate fibres, green; OT, optic tract; RG, retinogeniculate fibres, red; TC, thalamocortical fibres, purple). B, example currents of a silent (black) and a non-silent RG fibre (green) from P9–11 mice. NMDAR- and AMPAR-mediated currents were recorded at holding potentials of +40 and  $-70$  mV, respectively. C, quantification of silent fibres in wild-type and CKAMP44<sup>-/-</sup> mice ( $N = 12$  wild-type and 14 CKAMP44<sup>-/-</sup> mice; median and IQR). D, AMPA/NMDA ratio of retinogeniculate synaptic responses, including ( $N = 12$  wild-type and  $N = 14$  CKAMP44<sup>-/-</sup> mice, median and IQR) and excluding silent fibres ( $N = 12$  wild-type and  $N = 14$  CKAMP44<sup>-/-</sup> mice, mean  $\pm$  SD). [Colour figure can be viewed at wileyonlinelibrary.com]



**CKAMP44 augments short-term depression in retinogeniculate synapses**

We had previously shown that CKAMP44 increases short-term depression in retinogeniculate synapses of adult mice by slowing the recovery from desensitisation of AMPA receptors (Chen et al., 2018). To investigate whether CKAMP44 exerts a similar influence during development, we first analysed gating properties by inducing AMPAR-mediated currents with fast application of glutamate onto nucleated patches of relay neurons from wild-type and CKAMP44<sup>-/-</sup> mice (Fig. 5A). Deletion of CKAMP44 decreased peak current amplitudes of AMPAR-mediated currents for 1 ms glutamate pulses (median [IQR]: 98.02 [56.33–109.9] vs. 59.99 [36.97–87.05] pA, Mann–Whitney test:  $P = 0.0243$ ;  $n = 22$  wild-type and 23 CKAMP44<sup>-/-</sup> nucleated patches from  $N = 3$  wild-type and  $N = 3$  CKAMP44<sup>-/-</sup> mice) (Fig. 5B) suggesting that the number of extrasynaptic

AMPA receptors is reduced in relay neurons of CKAMP44<sup>-/-</sup> mice. In addition, CKAMP44 deletion increased the rate of recovery from desensitisation of AMPARs (decrease in the weighted  $\tau_{\text{recovery}}$ ) (Wild-type: 486.9 [433.6–525.6] ms,  $n = 19$  nucleated patches,  $N = 3$  mice; CKAMP44<sup>-/-</sup>: 48.02 [34.97–64.43] ms,  $n = 22$  nucleated patches,  $N = 3$  mice, Mann–Whitney test:  $P \leq 0.0001$ , median [IQR]) (Fig. 5C). Rise time and rates of deactivation and desensitisation were not affected by deletion of CKAMP44 (data not shown).

AMPA receptor kinetics and in particular the recovery from desensitisation is crucial for short-term depression in retinogeniculate synapses (Chen et al., 2018). We therefore investigated the role of CKAMP44 in short-term depression of young mice. Paired-pulse ratios of currents evoked with inter-pulse intervals of 30, 100 and 300 ms were increased in retinogeniculate synapses of CKAMP44<sup>-/-</sup> mice when compared to wild-type mice

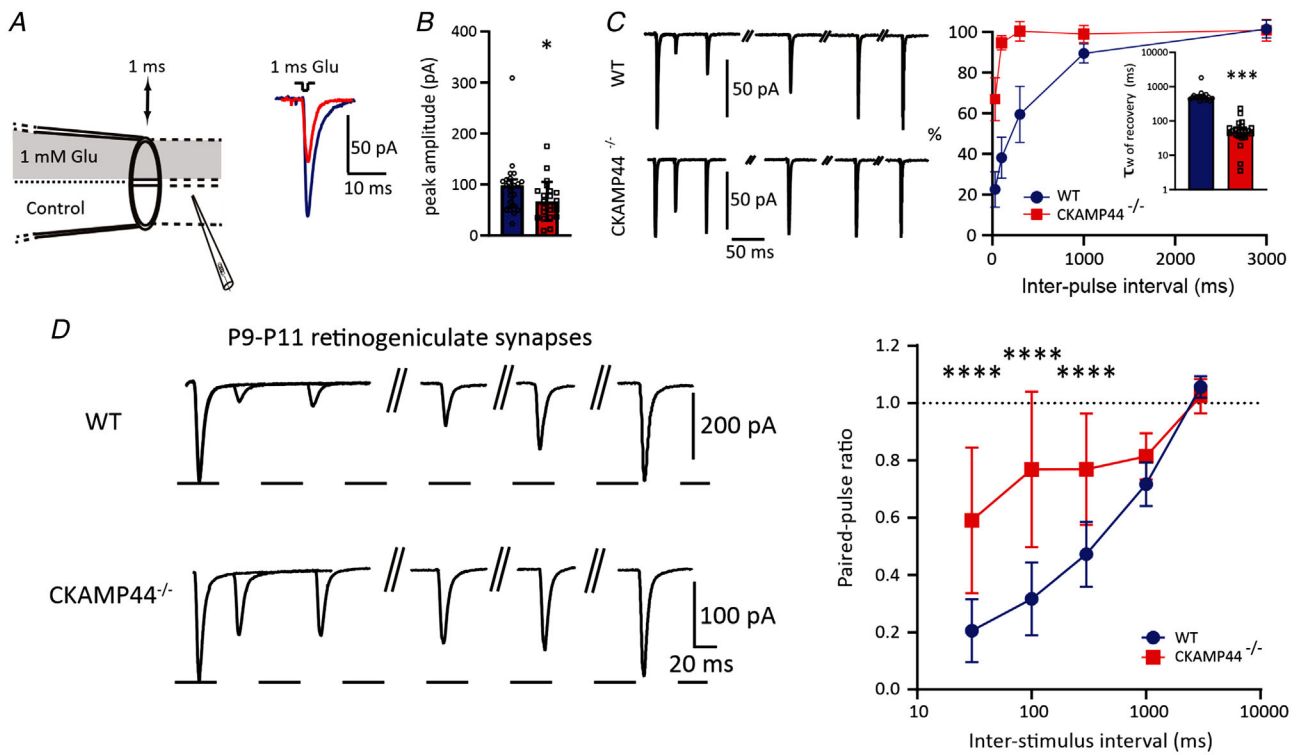


**Figure 5. CKAMP44 modulates gating properties of AMPARs and short-term plasticity in P9–11 mice**  
 A, schematic representation of nucleated patch experiments. B, quantification of peak amplitude of extrasynaptic AMPAR-mediated currents evoked by 1 ms glutamate pulses ( $n = 22$  and 23 relay neurons of  $N = 3$  control and  $N = 3$  CKAMP44<sup>-/-</sup> mice, respectively, median and IQR). Example traces are shown on the left. C, quantification of the amplitude of the second current as a percentage of the amplitude of the first current. The weighted time constant of recovery from desensitisation ( $\tau_{w \text{ of recovery}}$ ) was estimated from a double-exponential fit of the data. Example traces of pairs of currents that were evoked with two glutamate 1 ms pulses with different inter-pulse intervals (30, 100, 300, 1000 and 3000 ms) are shown on the left ( $n = 22$  and 23 relay neurons of  $N = 3$  control and  $N = 3$  CKAMP44<sup>-/-</sup> mice, respectively). Current percentage data are mean  $\pm$  SD,  $\tau_{w \text{ of recovery}}$  data are median and IQR). D, paired-pulse ratios of AMPAR-mediated currents evoked with extracellular stimulation of retinogeniculate synapses with different inter-pulse intervals (30, 100, 300, 1000 and 3000 ms,  $n = 22$  and 39 relay neurons of  $N = 3$  control and  $N = 6$  CKAMP44<sup>-/-</sup> mice, respectively, right panel, mean  $\pm$  SD). Examples of pairs of currents for the different inter-pulse intervals are shown on the left. [Colour figure can be viewed at wileyonlinelibrary.com]

(Wild-type, 30 ms:  $0.20555 \pm 0.10989$ ; CKAMP44<sup>-/-</sup>, 30 ms:  $0.59056 \pm 0.254344$ ,  $P \leq 0.0001$ ; wild-type, 100 ms:  $0.31673 \pm 0.12704$ ; CKAMP44<sup>-/-</sup>, 100 ms:  $0.76804 \pm 0.27173$ ,  $P \leq 0.0001$ ; wild-type, 300 ms:  $0.47240 \pm 0.11342$ ; CKAMP44<sup>-/-</sup>, 300 ms:  $0.76903 \pm 0.19426$ ,  $P \leq 0.0001$ ; wild-type, 1000 ms:  $0.71645 \pm 0.00554$ ; CKAMP44<sup>-/-</sup>, 1000 ms:  $0.81809 \pm 0.04693$ ,  $P = 0.4665$ ; wild-type, 3000 ms:  $1.05634 \pm 0.02729$ ; CKAMP44<sup>-/-</sup>, 3000 ms:  $1.02515 \pm 0.02957$ ,  $P = 0.9994$  [wild-type:  $n = 22$  relay neurons,  $N = 3$  mice; CKAMP44<sup>-/-</sup>:  $n = 39$  relay neurons,  $N = 6$  mice, one-way ANOVA, mean  $\pm$  SD]) (Fig. 5D).

In conclusion, deletion of CKAMP44 affects AMPAR gating and short-term plasticity in retinogeniculate synapses.

### The probability of inducing L-type Ca<sup>2+</sup> channel-mediated plateau potentials is increased in CKAMP44<sup>-/-</sup> mice

The strength of retinogeniculate synapses is significantly reduced in developing CKAMP44<sup>-/-</sup> mice indicating that deletion of CKAMP44 might also reduce the

probability of inducing plateau potentials. However, in adult CKAMP44<sup>-/-</sup> mice short-term depression is affected with increased paired-pulse ratio in retinogeniculate synapses due to a faster recovery from desensitisation of AMPARs (Chen et al., 2018). The weaker short-term depression increased spiking probability of dLGN neurons in CKAMP44<sup>-/-</sup> mice especially when retinogeniculate synapses were active at high frequencies (Chen et al., 2018). Considering that CKAMP44 is expressed in retinogeniculate synapses during development, one can assume that CKAMP44 also promotes short-term depression in retinogeniculate synapses of young mice. In this case, the probability of inducing plateau potentials may be increased in CKAMP44<sup>-/-</sup> mice despite the decreased AMPAR number at the retinogeniculate synapse. To induce plateau potentials, the optic tract was stimulated in acute brain slices of P9–11 mice at 50 Hz and voltage responses were recorded from relay neurons (Fig. 6A).

The probability of inducing plateau potentials was significantly increased in CKAMP44<sup>-/-</sup> mice compared to the probability in control mice (Wild-type:  $18.57 \pm 21.74\%$ ,  $N = 7$  mice; CKAMP44<sup>-/-</sup>:  $53.75 \pm 34.11\%$ ,  $N = 8$  mice,  $t$ -test:  $P = 0.0360$ , mean  $\pm$  SD) (Fig. 6B).

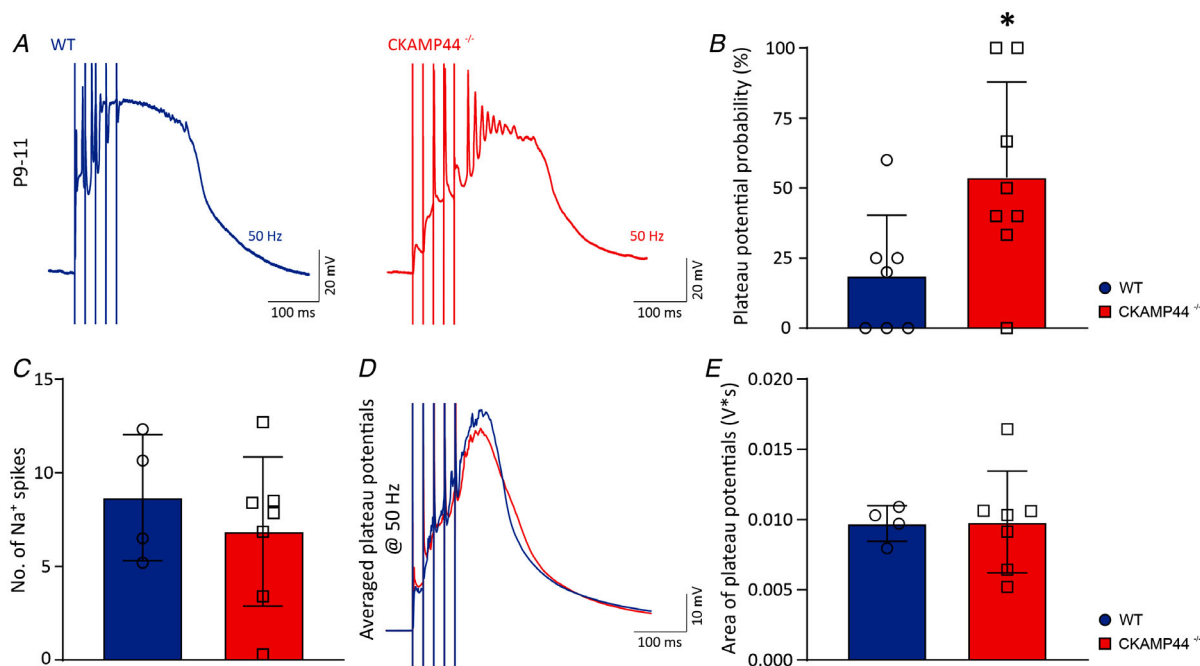


**Figure 6. CKAMP44 deletion increases the probability of eliciting L-type Ca<sup>2+</sup> channel-mediated plateau potentials**

A, example traces highlighting the characteristic appearance of L-type Ca<sup>2+</sup> channel-mediated plateau potentials in relay neurons of P9–11 wild-type and CKAMP44<sup>-/-</sup> mice (note: long-lasting depolarisation of high amplitude, inactivating sodium spikes, slow decay, stimulation frequency = 50 Hz). B, quantification of the probability with which plateau potentials could be elicited per animal ( $N = 7$  wild-type and  $N = 8$  CKAMP44<sup>-/-</sup> mice, mean  $\pm$  SD). C, quantification of sodium spikes elicited during plateau potentials ( $N = 4$  and  $7$  wild-type and CKAMP44<sup>-/-</sup> mice, mean  $\pm$  SD). D, averaged traces of plateau potentials from  $N = 4$  wild-type and  $N = 7$  CKAMP44<sup>-/-</sup> mice. E, quantification of the area of evoked plateau potentials ( $N = 4$  wild-type and  $N = 7$  CKAMP44<sup>-/-</sup> mice, mean  $\pm$  SD). [Colour figure can be viewed at [wileyonlinelibrary.com](http://wileyonlinelibrary.com)]

However, the induced plateau potentials did not differ between genotypes with similar numbers of inactivating sodium spikes during the plateau (Wild-type:  $8.67 \pm 3.37$  spikes,  $N = 4$  mice; CKAMP44<sup>-/-</sup>:  $6.86 \pm 3.98$  spikes,  $N = 7$  mice, *t*-test:  $P = 0.4648$ , mean  $\pm$  SD) (Fig. 6C) and unchanged areas of plateau potentials (Wild-type:  $0.009716 \pm 0.001268$  V\*s,  $N = 4$  mice; CKAMP44<sup>-/-</sup>:  $0.009821 \pm 0.003621$  V\*s,  $N = 7$  mice, *t*-test:  $P = 0.9572$ , mean  $\pm$  SD) (Fig. 6D and E). Increasing the stimulation frequency to 100 Hz did not increase the probability of inducing plateau potentials in wild-type and CKAMP44<sup>-/-</sup> mice (data not shown). In conclusion, loss of CKAMP44 facilitates the generation of L-type Ca<sup>2+</sup> channel-mediated plateau potentials.

### Loss of CKAMP44 does not alter retinal input segregation in the dLGN of young mice

Since loss of CKAMP44 increased the probability of L-type Ca<sup>2+</sup> channel-mediated plateau potentials, we

investigated whether input segregation is affected in the dLGN of CKAMP44<sup>-/-</sup> mice. Anterograde labelling of retinal ganglion cell axons by intravitreal injection of cholera toxin B (CTB) subunit conjugated to Alexa Fluor 488 (green) and Alexa Fluor 594 (red) into the right eye and left eye of P9–11 wild-type and CKAMP44<sup>-/-</sup> mice was used to analyse input segregation (Fig. 7A).

A threshold-independent method developed by Torborg & Feller (2004) was employed to analyse the axonal projections to the dLGN. The logarithm of the ratio of fluorescence intensities of the dyes from the ipsilateral and contralateral eye ( $R = \log [F_I/F_C]$ ) was calculated to determine *R* variance. High values of *R* variance, for instance, reflect strong segregation of inputs from left and right eye. Our analysis revealed similar variances in the *R* distribution (Wild-type:  $0.3854 \pm 0.0280$ ,  $N = 3$  mice; CKAMP44<sup>-/-</sup>:  $0.3646 \pm 0.0208$ ,  $N = 4$  mice, *t*-test:  $P = 0.6065$ , mean  $\pm$  SD) in the dLGN of wild-type and CKAMP44<sup>-/-</sup> mice (Fig. 7B and C). This indicates that eye-specific segregation is not affected by loss of CKAMP44.

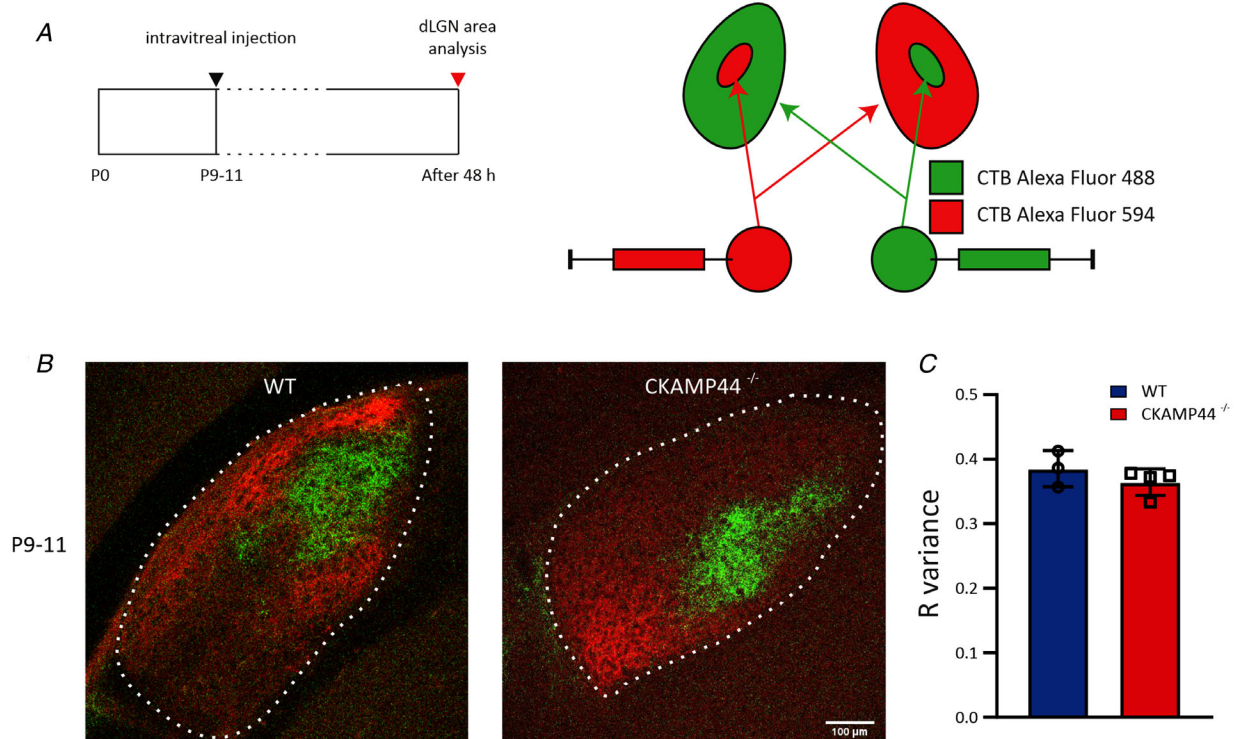


**Figure 7. Eye-specific segregation in dLGN of wild-type and CKAMP44<sup>-/-</sup> mice is unaltered**

A, illustration of the experimental procedures for anterograde labelling of retinal ganglion cell axons. Mice were injected at P9–11 and tissues harvested 48 h after injection and further processed for imaging. B, representative coronal slices containing the right dLGN of wild-type and CKAMP44<sup>-/-</sup> mice (P9–11 at the day of injection). The green and red fluorescence signals come from CTB-conjugated Alexa Fluor 488 and Alexa Fluor 594 that were injected into the ipsilateral eye and contralateral eye, respectively. Area of the dLGN marked by dashed lines. Fluorescence intensities for CTB–Alexa 488 and 594 were adjusted using the look-up table provided by the Leica TCS SP5 acquisition software to avoid under- or overexposure of images. Laser intensities were adjusted accordingly. C, quantification of *R* variance as a measure of input segregation (P9–11:  $N = 3$  and  $N = 4$  for wild-type and CKAMP44<sup>-/-</sup> mice, respectively; mean  $\pm$  SD). [Colour figure can be viewed at [wileyonlinelibrary.com](http://wileyonlinelibrary.com)]

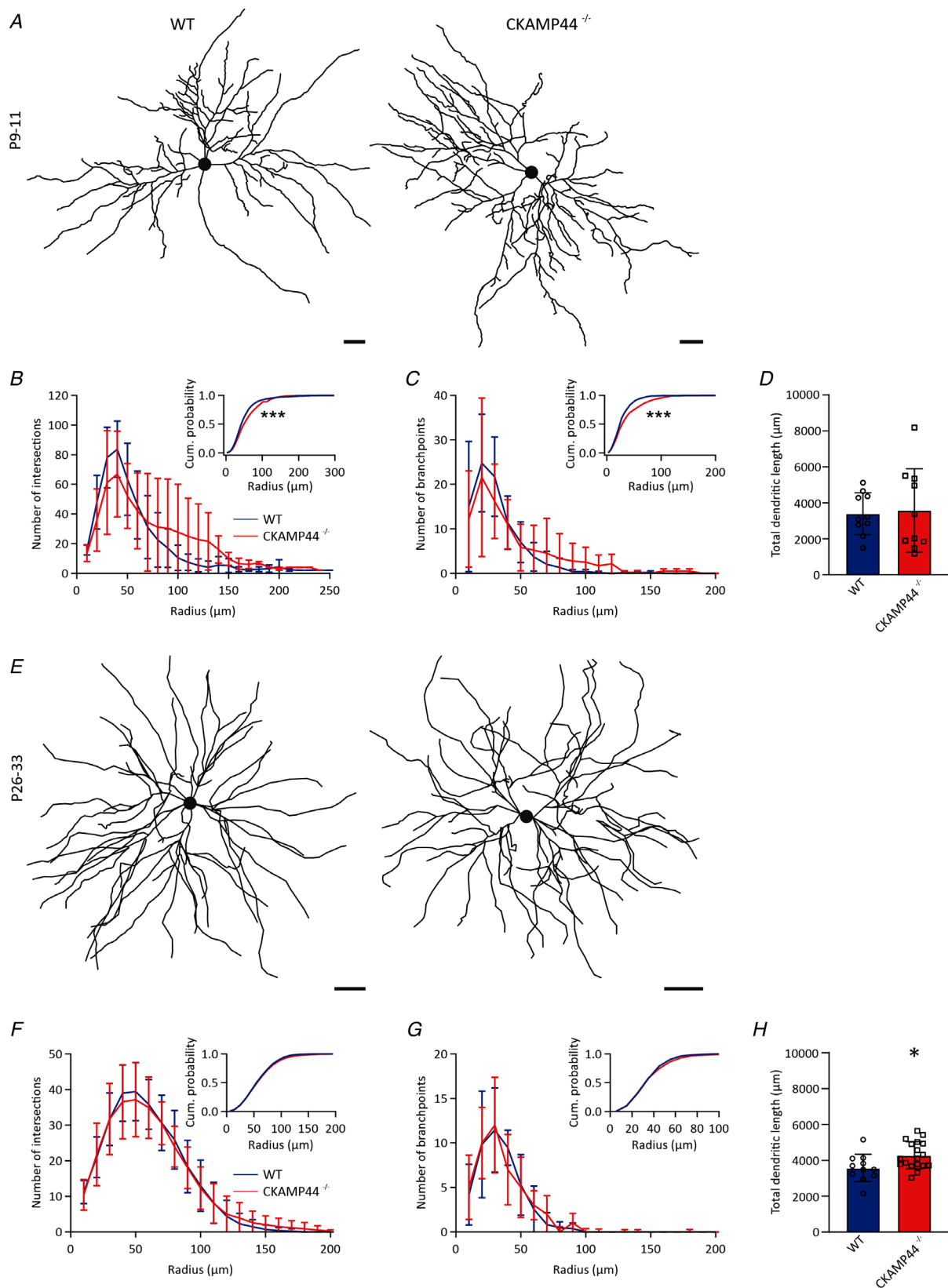


**Figure 8.** The anatomy of dLGN relay neurons is altered in CKAMP44<sup>-/-</sup> mice

A, examples of tracings of dLGN neurons from P9–11 mice (scale bar, 10 μm). B and C, number of dendritic intersections (B) and branch points (C) of relay neurons of P9–11 wild-type and CKAMP44<sup>-/-</sup> mice. Inset in B and

C, cumulative distributions of intersections and branch points, respectively. D, total dendritic length of relay neurons of P9–11 wild-type and CKAMP44<sup>-/-</sup> mice. (B–D:  $n = 10$  and 10 relay neurons from recordings of  $N = 4$  wild-type and  $N = 6$  CKAMP44<sup>-/-</sup> mice, respectively, mean  $\pm$  SD.) E, examples of tracings of dLGN neurons from P26–33 mice (scale bar, 20  $\mu$ m). F and G, number of dendritic intersections (F) and branch points (G) of relay neurons of P26–33 wild-type and CKAMP44<sup>-/-</sup> mice. Inset in F and G, cumulative distributions of intersections and branch points, respectively. H, total dendritic length of relay neurons of P26–33 wild-type and CKAMP44<sup>-/-</sup> mice. (F–H:  $n = 11$  and 18 relay neurons of  $N = 6$  wild-type and  $N = 11$  CKAMP44<sup>-/-</sup> mice, respectively, mean  $\pm$  SD.) P9–11 data obtained from animals used for plateau potential analysis. [Colour figure can be viewed at [wileyonlinelibrary.com](http://wileyonlinelibrary.com)]

### Lack of CKAMP44 alters branching of relay neurons during early dLGN development

Absence of excitatory input from retinal ganglion cells to the dLGN can cause a period of exuberant branching in relay neurons throughout postnatal week 2 (El-Danaf et al., 2015). The reduction of synaptic strength in CKAMP44<sup>-/-</sup> mice may also alter relay neuron morphology. Thus, Sholl analysis on biocytin-filled reconstructed relay neurons of young mice was performed, which revealed changes in dendritic arborisation in dLGN relay neurons of P9–11 CKAMP44<sup>-/-</sup> mice. Cumulative distribution of the number of dendritic intersections (KS test:  $P < 0.00001$ ) and branch points (KS test:  $P < 0.00001$ ) was significantly increased in CKAMP44<sup>-/-</sup> mice (Fig. 8B and C inset) while total dendritic length (Wild-type:  $3398 \pm 1166 \mu\text{m}$ ,  $n = 10$  relay neurons,  $N = 4$  mice; CKAMP44<sup>-/-</sup>:  $3580 \pm 2318 \mu\text{m}$ ,  $n = 10$  relay neurons,  $N = 6$  mice,  $t$ -test:  $P = 0.8269$ , mean  $\pm$  SD) was unaffected (Fig. 8D). The branching of relay neuron dendrites in mice with absence of excitatory input from retinal ganglion cells normalised in the third postnatal week (El-Danaf et al., 2015). Similarly, in P26–33 CKAMP44<sup>-/-</sup> mice dendritic branching of relay neurons was not different from branching in wild-type mice. Cumulative distribution of the number of dendritic intersections (KS test:  $P = 0.2133$ ) and branch points (KS test:  $P = 0.657$ ) was comparable to wild-type neurons in CKAMP44<sup>-/-</sup> mice (Fig. 8F and G inset) while total dendritic length (Wild-type:  $3583 \pm 765 \mu\text{m}$ ,  $n = 11$  relay neurons,  $N = 6$  mice; CKAMP44<sup>-/-</sup>:  $4283 \pm 756 \mu\text{m}$ ,  $n = 18$  relay neurons,  $N = 11$  mice,  $t$ -test:  $P = 0.0230$ , mean  $\pm$  SD) was increased (Fig. 8H).

### Discussion

AMPA function depends on auxiliary subunits (TARPs, CKAMPs, cornichons and GSG1L) (Jacobi & von Engelhardt, 2018). CKAMP44, a member of the CKAMP family (Farrow et al., 2015), has previously been identified as an auxiliary subunit of AMPARs that promotes receptor surface trafficking, synapse targeting and modulates receptor gating properties in dLGN relay neurons (Chen et al., 2018). Here we investigated the role of CKAMP44 in dLGN in retinogeniculate synapse function during early postnatal development. We showed that CKAMP44 is

stably expressed throughout development and influences AMPAR-mediated currents in young (this study) and adult mice (Chen et al., 2018). Genetic deletion of CKAMP44 decreases synaptic strength, increases the proportion of silent fibres and the probability of inducing plateau potentials. Development of neuron morphology was mildly affected but input segregation was not altered in CKAMP44<sup>-/-</sup> mice.

The development of the visual system is a complex process that includes pruning of weak synapses, which are initially formed between retinal ganglion cells and dLGN relay neurons (Chen & Regehr, 2000; Huberman, 2007), the strengthening of remaining connections by increasing the number of release sites and the number of AMPARs per synapse (Chen & Regehr, 2000), and local clustering of axonal boutons at the same dendritic domains (Liang et al., 2018). The claim that only one or two retinal inputs per relay neuron remain has recently been challenged (Hammer et al., 2015; Rompani et al., 2017). Even though there are more convergent inputs present than initially thought, most of these inputs seem to have a modulatory role and only a third are actually driving relay neurons to fire action potentials (Litvina & Chen, 2017a). While the development and anatomical details of retinal inputs in the dLGN has extensively been studied (Guido, 2018; Litvina & Chen, 2017b), further research concerning the molecular mechanisms governing these processes is needed.

Previously, it has been shown that upregulation of the auxiliary protein TARP  $\gamma$ -2 contributes to the developmental increase in synaptic AMPAR expression (Louros et al., 2014). TARP  $\gamma$ -4 is another auxiliary subunit that is expressed in the dLGN (Louros et al., 2014), but its role in AMPAR modulation in this brain area is so far unclear. Here we identify CKAMP44 as an AMPAR-auxiliary protein that is expressed early during development (at least from P5–7 on) and that, consistent with its stable expression, influences AMPAR function at the investigated developmental time points and in adult mice (Chen et al., 2018). Considering the magnitude of changes in AMPA/NMDA ratios in the respective knockout mice (this study) and other studies (Chen et al., 2018; Louros et al., 2014), CKAMP44 and TARP  $\gamma$ -2 are two main auxiliary proteins controlling AMPAR number and function in the dLGN. By FISH we showed that *Shisa9* mRNA (encoding CKAMP44) is expressed

not only in relay neurons, but also in GABAergic interneurons of the dLGN. Interneurons migrate from the ventral lateral geniculate nucleus (vLGN) into the dLGN during the first two postnatal weeks and only a few interneurons are detected within the most superficial layer of the dLGN during the first postnatal week (Golding et al., 2014). Consistently, we detected no *Gad1* mRNA signal in P5–7 mice. Thereafter, *Shisa9* mRNA expression was stable in GABAergic interneurons throughout development similar to non-GABAergic relay neurons even though the CKAMP44 mRNA expression level was lower in GABAergic interneurons than in non-GABAergic relay neurons. The functional role of CKAMP44 in dLGN interneurons remains to be investigated.

Deletion of CKAMP44 decreases mEPSC frequency and AMPA/NMDA ratio suggesting that silent synapse number is increased in relay neurons of P9–11 CKAMP44<sup>-/-</sup> mice. Indeed, minimal stimulation experiments revealed a doubling of silent retinogeniculate fibre number in relay neurons of P9–11 CKAMP44<sup>-/-</sup> mice. Unsilencing of silent synapses is an important step in the process of visual system maturation contributing to the strengthening of retinogeniculate connections together with the addition of more AMPARs to existing synapses and the establishment of new release sites (Chen & Regehr, 2000). The unsilencing process is controlled by pentraxins, which are presynaptically released by retinal ganglion cells and cluster AMPARs at the postsynaptic site on dLGN relay neurons (Koch & Ullian, 2010). Auxiliary subunits such as the proteins of the CKAMP and TARP families, which promote trafficking of AMPARs to the cell surface and enable their anchoring in the synapses (Chen et al., 2000; von Engelhardt et al., 2010), are good candidates for mediating the unsilencing of silent synapses. Proteins of both families harbour PDZ domain binding motifs at their C-termini that allow stabilisation of AMPARs within the synapse via interaction with membrane-associated guanylate kinases (MAGUKs) such as PSD95 (Farrow et al., 2015; Khodosevich et al., 2014; Tomita et al., 2003). A recent study by Harb et al. demonstrated that TARP  $\gamma$ -8 and CKAMP44 reduce the internalization rate of extrasynaptic surface receptors and thus delay local recycling and increase surface lifetime of GluA1-containing AMPARs in cultured neurons (Harb et al., 2021). Our findings suggest that CKAMP44 unsilences and strengthens retinogeniculate synapses during development of the dLGN through increased insertion of AMPARs at the postsynaptic site on dLGN relay neurons. Deletion of CKAMP44 decreases mEPSC amplitude also in P5–7 mice consistent with reduced synaptic AMPAR number. However, mEPSC frequency was not decreased in P5–7 CKAMP44<sup>-/-</sup> mice, suggesting that the reduction in AMPAR number is more homogeneous than in P9–11 CKAMP44<sup>-/-</sup> mice. Developmental changes in the AMPAR complex with

altered contribution of other auxiliary subunits such as TARP  $\gamma$ -2 (Louros et al., 2014) may influence the effect of CKAMP44 deletion at the different ages.

Some of the observed changes in retinogeniculate synapse function in CKAMP44<sup>-/-</sup> mice could result from alterations in retinal activity. For example, the reduction in mEPSC frequency and increase in paired-pulse ratios in relay neurons of P9–11 CKAMP44<sup>-/-</sup> mice could be explained by a reduction in vesicle release probability in retinogeniculate synapses. However, this would not explain the reduced AMPA/NMDA ratio and increased silent fibre number in minimal stimulation experiments. Moreover, we previously demonstrated in brain slices of adult mice that CKAMP44 deletion increases paired-pulse ratios of synaptic currents by slowing recovery from desensitisation of AMPARs and not by decreasing vesicle release probability (Khodosevich et al., 2014; von Engelhardt et al., 2010). Finally, unaltered synaptic currents in retinal ganglion cells and normal electroretinograms in CKAMP44<sup>-/-</sup> mice suggested that deletion of CKAMP44 has no major influence on retinal function (Chen et al., 2018). We therefore conclude that the alterations in retinogeniculate synapse function in CKAMP44<sup>-/-</sup> mice result most likely from absence of CKAMP44 in relay neurons and not from changes in the function of neurons that project to the dLGN.

Loss of CKAMP44 was also accompanied by a transient change in dendritic arborisation of dLGN relay neurons that resembled earlier findings from a study of *math5*<sup>-/-</sup> mice (El-Danaf et al., 2015). Genetic deletion of *math5* caused loss of retinal ganglion cells and their axonal innervation. This resulted in exuberant dendritic branching of relay neurons in the second postnatal week with an increase in higher-order branch number. In our study a similar shift in dendritic branching was seen which might be attributed to a reduction in excitatory drive. The effect was also only transient and could not be seen in older P26–33 CKAMP44<sup>-/-</sup> mice. As was suggested by El-Danaf et al., regulation of dendritic arborisation might be controlled by descending corticogeniculate projections to the dLGN in older mice. Thus, our findings highlight a critical period of development in which CKAMP44 might control dendritic branching by its effect on synapse function and strength.

Eye-specific segregation requires spontaneous spiking activity in the retina (Shatz & Stryker, 1988; Sretavan et al., 1988), and the structure of this activity is thought to instruct synaptic competition in the dLGN (Muir-Robinson et al., 2002; Penn et al., 1998; Rossi et al., 2001; Stellwagen & Shatz, 2002). The changes in AMPAR-mediated currents with reduced synaptic strength and altered short-term depression in CKAMP44<sup>-/-</sup> mice prompted us to test, whether deletion of CKAMP44 affects input segregation. Several explanations may account for the fact that this is

not the case. The reduction in synaptic strength by loss of CKAMP44 might be too small to negatively influence input segregation. More importantly, changes in short-term plasticity may in fact cause a more pronounced depolarisation in CKAMP44<sup>-/-</sup> mice than in wild-type mice when retinal ganglion cells fire with frequencies of >10 Hz despite the fact that the number of AMPARs is reduced (Chen et al., 2018). Indeed, the probability of inducing plateau potentials is increased in CKAMP44<sup>-/-</sup> mice. This can be explained by a stronger depolarisation of relay cells in CKAMP44<sup>-/-</sup> mice than in wild-type mice due to the fast recovery from desensitisation of AMPARs that do not interact with CKAMP44 and consequently the decreased paired-pulse depression of synaptic currents. Plateau potentials were shown to positively influence input segregation and drive synapse refinement during the first postnatal weeks (Dilger et al., 2015; Lo et al., 2002). Thus, the higher probability of inducing plateau potentials in CKAMP44<sup>-/-</sup> mice could explain normal input segregation despite the reduction in synapse strength.

In conclusion, we demonstrate that CKAMP44 controls synapse function and strength of relay neurons but is not essential for normal development of the dLGN.

## References

- Chen, C., & Regehr, W. G. (2000). Developmental remodeling of the retinogeniculate synapse. *Neuron*, **28**(3), 955–966.
- Chen, L., Chetkovich, D. M., Petralia, R. S., Sweeney, N. T., Kawasaki, Y., Wenthold, R. J., Brecht, D. S., & Nicoll, R. A. (2000). Stargazin regulates synaptic targeting of AMPA receptors by two distinct mechanisms. *Nature*, **408**(6815), 936–943.
- Chen, X., Aslam, M., Gollisch, T., Allen, K., & von Engelhardt, J. (2018). CKAMP44 modulates integration of visual inputs in the lateral geniculate nucleus. *Nature Communication*, **9**(1), 261.
- Chen, X. F., Wang, D. N., Kegel, M., & von Engelhardt, J. (2019). Electrophysiological Investigations of retinogeniculate and corticogeniculate synapse function. *Journal of Visualized Experiments*, (150), doi: 10.3791/59680.
- Dilger, E. K., Krahe, T. E., Morhardt, D. R., Seabrook, T. A., Shin, H. S., & Guido, W. (2015). Absence of plateau potentials in dLGN cells leads to a breakdown in retinogeniculate refinement. *Journal of Neuroscience*, **35**(8), 3652–3662.
- El-Danaf, R. N., Krahe, T. E., Dilger, E. K., Bickford, M. E., Fox, M. A., & Guido, W. (2015). Developmental remodeling of relay cells in the dorsal lateral geniculate nucleus in the absence of retinal input. *Neural Development*, **10**(1), 19.
- Farrow, P., Khodosevich, K., Sapir, Y., Schulmann, A., Aslam, M., Stern-Bach, Y., Monyer, H., & von Engelhardt, J. (2015). Auxiliary subunits of the CKAMP family differentially modulate AMPA receptor properties. *eLife*, **4**, e09693.
- Golding, B., Pouchelon, G., Bellone, C., Murthy, S., Di Nardo, A. A., Govindan, S., Ogawa, M., Shimogori, T., Luscher, C., Dayer, A., & Jabaudon, D. (2014). Retinal input directs the recruitment of inhibitory interneurons into thalamic visual circuits. *Neuron*, **81**(5), 1057–1069.
- Grundy, D. (2015). Principles and standards for reporting animal experiments in *The Journal of Physiology* and *Experimental Physiology*. *Journal of Physiology*, **593**(12), 2547–2549.
- Guido, W. (2018). Development, form, and function of the mouse visual thalamus. *Journal of Neurophysiology*, **120**(1), 211–225.
- Hammer, S., Monavafeshani, A., Lemon, T., Su, J., & Fox, M. A. (2015). Multiple retinal axons converge onto relay cells in the adult mouse thalamus. *Cell Reports*, **12**(10), 1575–1583.
- Harb, A., Vogel, N., Shaib, A., Becherer, U., Bruns, D., & Mohrmann, R. (2021). Auxiliary subunits regulate the dendritic turnover of AMPA receptors in mouse hippocampal neurons. *Frontiers in Molecular Neuroscience*, **14**, 728498.
- Hooks, B. M., & Chen, C. F. (2006). Distinct roles for spontaneous and visual activity in remodeling of the retinogeniculate synapse. *Neuron*, **52**(2), 281–291.
- Huberman, A. D. (2007). Mechanisms of eye-specific visual circuit development. *Current Opinion in Neurobiology*, **17**(1), 73–80.
- Huberman, A. D., Feller, M. B., & Chapman, B. (2008). Mechanisms underlying development of visual maps and receptive fields. *Annual Review of Neuroscience*, **31**(1), 479–509.
- Jacobi, E., & von Engelhardt, J. (2017). Diversity in AMPA receptor complexes in the brain. *Current Opinion in Neurobiology*, **45**, 32–38.
- Jacobi, E., & von Engelhardt, J. (2018). AMPA receptor complex constituents: Control of receptor assembly, membrane trafficking and subcellular localization. *Molecular and Cellular Neuroscience*, **91**, 67–75.
- Khodosevich, K., Jacobi, E., Farrow, P., Schulmann, A., Rusu, A., Zhang, L., Sprengel, R., Monyer, H., & von Engelhardt, J. (2014). Coexpressed auxiliary subunits exhibit distinct modulatory profiles on AMPA receptor function. *Neuron*, **83**(3), 601–615.
- Koch, S. M., & Ullian, E. M. (2010). Neuronal pentraxins mediate silent synapse conversion in the developing visual system. *Journal of Neuroscience*, **30**(15), 5404–5414.
- Liang, L., Fratzl, A., Goldey, G., Ramesh, R. N., Sugden, A. U., Morgan, J. L., Chen, C., & Andermann, M. L. (2018). A fine-scale functional logic to convergence from retina to thalamus. *Cell*, **173**(6), 1343–1355.e24.
- Litvina, E. Y., & Chen, C. (2017a). Functional convergence at the retinogeniculate synapse. *Neuron*, **96**(2), 330–338.e5.
- Litvina, E. Y., & Chen, C. (2017b). An evolving view of retinogeniculate transmission. *Visual Neuroscience*, **34**, E013.
- Lo, F. S., Ziburkus, J., & Guido, W. (2002). Synaptic mechanisms regulating the activation of a Ca<sup>2+</sup>-mediated plateau potential in developing relay cells of the LGN. *Journal of Neurophysiology*, **87**(3), 1175–1185.

- Louros, S. R., Hooks, B. M., Litvina, L., Carvalho, A. L., & Chen, C. (2014). A role for stargazin in experience-dependent plasticity. *Cell Reports*, **7**(5), 1614–1625.
- Muir-Robinson, G., Hwang, B. J., & Feller, M. B. (2002). Retinogeniculate axons undergo eye-specific segregation in the absence of eye-specific layers. *Journal of Neuroscience*, **22**(13), 5259–5264.
- Muller, M. K., Jacobi, E., Sakimura, K., Malinow, R., & von Engelhardt, J. (2018). NMDA receptors mediate synaptic depression, but not spine loss in the dentate gyrus of adult amyloid Beta (A beta). overexpressing mice. *Acta Neuro-pathologica Communications*, **6**(1), 110.
- Paxinos, G., & Franklin, K. B. J. (2012). *The mouse brain in stereotaxic coordinates* (4th ed.). Academic Press.
- Paxinos, G., Halliday, G., Koutcherov, Y., Wang, H., & Watson, C. (2006). *Atlas of the developing mouse brain at E17.5, P0 and P6* (1st ed.). Academic Press.
- Penn, A. A., Riquelme, P. A., Feller, M. B., & Shatz, C. J. (1998). Competition in retinogeniculate patterning driven by spontaneous activity. *Science*, **279**(5359), 2108–2112.
- Rompani, S. B., Mullner, F. E., Wanner, A., Zhang, C., Roth, C. N., Yonehara, K., & Roska, B. (2017). Different modes of visual integration in the lateral geniculate nucleus revealed by single-cell-initiated transsynaptic tracing. *Neuron*, **93**(4), 767–776.e6.
- Rossi, F. M., Pizzorusso, T., Porciatti, V., Marubio, L. M., Maffei, L., & Changeux, J. P. (2001). Requirement of the nicotinic acetylcholine receptor beta 2 subunit for the anatomical and functional development of the visual system. *Proceedings of the National Academy of Sciences, USA*, **98**(11), 6453–6458.
- Sather, W., Dieudonne, S., Macdonald, J. F., & Ascher, P. (1992). Activation and desensitization of n-methyl-d-aspartate receptors in nucleated outside-out patches from mouse neurons. *Journal of Physiology*, **450**(1), 643–672.
- Shatz, C. J., & Stryker, M. P. (1988). Prenatal Tetrodotoxin infusion blocks segregation of retinogeniculate afferents. *Science*, **242**(4875), 87–89.
- Sretavan, D. W., Shatz, C. J., & Stryker, M. P. (1988). Modification of retinal ganglion-cell axon morphology by prenatal infusion of tetrodotoxin. *Nature*, **336**(6198), 468–471.
- Stellwagen, D., & Shatz, C. J. (2002). An instructive role for retinal waves in the development of retinogeniculate connectivity. *Neuron*, **33**(3), 357–367.
- Tomita, S., Chen, L., Kawasaki, Y., Petralia, R. S., Wenthold, R. J., Nicoll, R. A., & Brecht, D. S. (2003). Functional studies and distribution define a family of transmembrane AMPA receptor regulatory proteins. *Journal of Cell Biology*, **161**(4), 805–816.
- Torborg, C. L., & Feller, M. B. (2004). Unbiased analysis of bulk axonal segregation patterns. *Journal of Neuroscience Methods*, **135**(1–2), 17–26.
- Torborg, C. L., Hansen, K. A., & Feller, M. B. (2005). High frequency, synchronized bursting drives eye-specific segregation of retinogeniculate projections. *Nature Neuroscience*, **8**(1), 72–78.
- Trcek, T., Larson, D. R., Moldon, A., Query, C. C., & Singer, R. H. (2011). Single-molecule mRNA decay measurements reveal promoter-regulated mRNA stability in yeast. *Cell*, **147**(7), 1484–1497.
- Turner, J. P., & Salt, T. E. (1998). Characterization of sensory and corticothalamic excitatory inputs to rat thalamocortical neurones in vitro. *Journal of Physiology*, **510**(3), 829–843.
- von Engelhardt, J., Mack, V., Sprengel, R., Kavenstock, N., Li, K. W., Stern-Bach, Y., Smit, A. B., Seeburg, P. H., & Monyer, H. (2010). CKAMP44: a brain-specific protein attenuating short-term synaptic plasticity in the dentate gyrus. *Science*, **327**(5972), 1518–1522.
- von Engelhardt, J., Doganci, B., Jensen, V., Hvalby, O., Gongrich, C., Taylor, A., Barkus, C., Sanderson, D. J., Rawlins, J. N., Seeburg, P. H., Bannerman, D. M., & Monyer, H. (2008). Contribution of hippocampal and extra-hippocampal NR2B-containing NMDA receptors to performance on spatial learning tasks. *Neuron*, **60**(5), 846–860.

## Additional information

### Data availability statement

The data of this manuscript are available from the corresponding author upon reasonable request.

### Competing interests

None.

### Author contributions

F.H., D.W., X.C., J.Z. and M.A.: acquisition of data. F.H., D.W., X.C., J.Z., M.A., H.T., F.G., and J.vE.: conception and design of the study, analysis and interpretation of data, drafting or revising the article. All authors have read and approved the final version of this manuscript and agree to be accountable for all aspects of the work in ensuring that questions related to the accuracy or integrity of any part of the work are appropriately investigated and resolved. All persons designated as authors qualify for authorship, and all those who qualify for authorship are listed.

### Funding

This work was funded by the German Research Foundation (DFG) grant within the Collaborative Research Centre (SFB) 1080 ‘Molecular and Cellular Mechanisms of Neural Homeostasis’ to J.vE.

### Acknowledgements

The authors want to thank Barbara Biesalski and Chiara Ardigo for excellent technical assistance.

Open Access funding enabled and organized by Projekt DEAL.



### Author's present address

Xufeng Chen, Stony Brook University Pain and Analgesia Research Centre (SPARC) and Anesthesiology, Renaissance School of Medicine, Stony Brook University, NY 11794, USA.

### Keywords

AMPA receptor, CKAMP44, dLGN, shisa9

### Supporting information

Additional supporting information can be found online in the Supporting Information section at the end of the HTML view of the article. Supporting information files available:

### Peer Review History

### Statistical Summary Document